APL Materials

RESEARCH ARTICLE | FEBRUARY 14 2024

Experimental investigation of Rayleigh wave propagation in a locally resonant metamaterial layer resting on an elastic half-space

Farhad Zeighami ; Antonio Palermo ; Denis Bogomolov ; Alessandro Marzani

APL Mater. 12, 021115 (2024)
https://doi.org/10.1063/5.0171532

Experimental investigation of Rayleigh wave propagation in a locally resonant metamaterial layer resting on an elastic half-space

Cite as: APL Mater. 12, 021115 (2024); doi: 10.1063/5.0171532
Submitted: 9 August 2023 • Accepted: 21 January 2024 •
Published Online: 14 February 2024

Farhad Zeighami,[1,a)] Antonio Palermo,[1,2] Denis Bogomolov,[2] and Alessandro Marzani[1,2]

AFFILIATIONS

[1] Department of Civil, Chemical, Environmental, and Materials Engineering - DICAM, University of Bologna, Viale del Risorgimento, 2, Bologna 40136, Italy
[2] Advanced Research Center on Electronic Systems "Ercole De Castro" (ARCES), University of Bologna, Viale Carlo Pepoli, 3/2, Bologna 40123, Italy

Note: This paper is part of the Special Topic on New Frontiers in Acoustic and Elastic Metamaterials and Metasurfaces.
[a)] **Author to whom correspondence should be addressed:** farhad.zeighami3@unibo.it

ABSTRACT

In this experimental investigation, we explore the propagation characteristics of surface Rayleigh waves in a Locally Resonant Metamaterial (LRM) layer positioned on an elastic half-space. The study focuses on characterizing the dispersion and attenuation properties of these waves and validating analytical and numerical models of the LRM. For practical purposes, we utilize a thin-plate sample and construct the LRM layer, featuring multiple rows of sub-wavelength resonators, by machining the resonators at one edge of the plate. Employing a piezoelectric transducer coupled to the plate and a laser vibrometer, we actuate and receive the surface-like waves propagating at the plate edge. Two resonant layer configurations, comprising 3 and 5 rows of resonators, corresponding to heights of $\sim 0.6\lambda_h$ and λ_h, where λ_h represents the reference wavelength of Rayleigh waves, are examined. The experimental observations reveal the hybridization of the fundamental surface mode at the resonant frequency of the embedded resonators, leading to the creation of a low-frequency bandgap. This bandgap, attributed to the local resonance mechanism, exhibits a remarkable attenuation of surface wave amplitudes. To support our experimental findings, we conduct both analytical and numerical studies. These analyses demonstrate the confinement of the lowest-order surface mode within the frequency ranges proximate to the resonators' resonance. The insights gained from this experimental study contribute to the advancement of strategies for mitigating surface waves through the application of resonant metamaterials and metastructures.

I. INTRODUCTION

Locally resonant metamaterials (LRMs) are artificial composite materials with extraordinary mechanical properties, such as zero or negative mass density[1,2] and negative bulk modulus,[3] which are induced by the material-specific microstructure. These unique characteristics have made LRMs a popular research topic over the past two decades and opened up the possibilities of using them for different engineering applications. LRMs are typically constructed by encasing resonant elements in a host medium.[1] The distributed local resonances create a narrow stop-band frequency region close to the resonant frequency of the resonators.[4] Within this specific frequency range, the propagation of waves is impeded, allowing LRMs to be used in a variety of applications where the attenuation of elastic waves is needed.

More recently, LRMs have been used to control the propagation of surface waves (SWs) traveling along the surface of a waveguide, such as the ground surface or the surface boundary of a solid material.[5,6] If their resonant frequency is tuned to match the frequency of incoming surface waves, they can be used as efficient surface wave filters.[7,8] Hence, LRMs have found multiple applications in the context of seismic surface wave mitigation[6,7,9] and

railway-induced vibration abatement systems.[10,11] Other applications for surface wave manipulation include wave guiding[12] and wave focusing.[13,14]

So far, most of the previous studies on the interaction of surface waves and LRMs have primarily focused on locally resonant metasurfaces. Such structured materials are generally composed of resonant units placed atop an elastic medium in a desired periodic or aperiodic pattern to form a thin (e.g., strongly sub-wavelength) resonant boundary.[7,8,15,16] For this reason, resonant metasurfaces are typically modeled as boundary conditions acting at the surface of the elastic waveguide.[5,7,8,17–20] During recent years, such resonant metasurfaces have found various applications in the design of surface wave barriers,[7] topological insulators,[21] and energy harvesters,[22–24] just to name a few.

Although the metasurface boundary-condition models are useful in certain applications, they are not able to correctly capture the interaction between surface waves and resonant structures with a depth comparable to the propagating wavelength, as in the case of mitigation systems for ground-borne vibrations. For such scenarios, a few numerical and experimental studies have been proposed.[25] For instance, an experimental investigation was recently performed by Zaccherini *et al.*[26] to study the dynamics of a metabarrier with multi-layer sub-wavelength resonators attached to a heterogeneous granular medium. Notably, in such a medium, multiple surface modes exist, the so-called guided surface acoustic modes, which can couple with the added metabarrier.

In parallel, we recently proposed an analytical formulation based on a homogenization technique[27] to investigate the dynamics of a multi-layer resonant barrier embedded within a homogeneous medium. In such a medium, only a fundamental surface mode, e.g., the Rayleigh wave, propagates and couples with the collective motion of the barrier. The proposed approach treats the resonant layer (RL) as an equivalent homogeneous layer with effective mechanical parameters. The equivalent layer is used to derive a closed-form dispersion law suitable to investigate deep barriers in the long-wavelength regime.

The objective of this work is to complement our previous analytical study by providing an experimental investigation of Rayleigh waves propagating in a layer of LRMs overlaying an elastic half-space (HS). To achieve this, we design and realize a resonant metamaterial layer composed of resonant unit cells arranged periodically within a hosting thin-plate. The use of thin plates as experimental platforms to explore the dynamics of surface waves in half-space media is justified by the similarity between Rayleigh waves and extensional waves propagating along the edge of a thin plate.[28,29] By using the laser Doppler vibrometry technique, we measure the wavefield of surface waves propagating along the resonant layer and characterize its dispersive features. To analyze the resonant frequency of the unit cell and calculate the effective parameters of the homogenized layer, we develop numerical finite element (FE) models. Finally, we compare the experimental results with those predicted by the analytical formulation and numerical models. This comparative analysis enables us to assess the accuracy and validity of the proposed dispersion formulation.

The remainder of the paper is structured as follows: Sec. II describes the problem of interest and the related experimental test setup; Sec. III presents the experimental results; and Sec. IV discusses the numerical and analytical models used to interpret the experimental findings. Finally, Sec. V concludes the paper and explores potential future applications of the LRMs to control the propagation of surface waves.

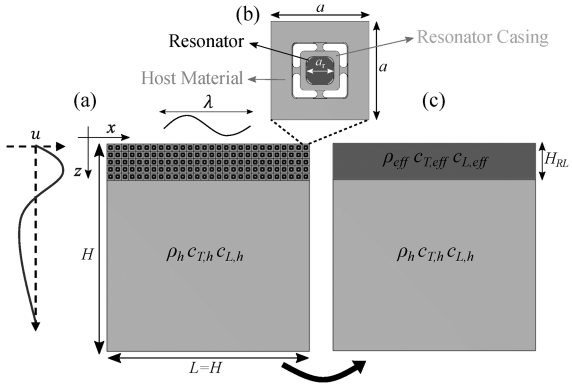

FIG. 1. Schematics of (a) a homogeneous and isotropic plate equipped with a resonant layer containing an array of resonators, (b) a unit cell, and (c) an equivalent homogenized layer with effective elastic parameters.

TABLE I. Material properties of the model parameters.

Parameter	Unit	PVC	Steel
Mass density (ρ)	kg/m^3	$\rho_h = 1470$	$\rho_r = 7850$
Elastic modulus (E)	GPa	$E_h = 4.15$	$E_r = 210$
Poisson's ratio (ν)	⋯	$\nu_h = 0.4$	$\nu_r = 0.3$

II. EXPERIMENTAL SETUP

We analyze the propagation of vertically polarized surface waves in a resonant layer consisting of multiple strata of embedded resonators coupled to an elastic half-space. For this purpose, we utilize a plate made of Polyvinyl chloride (PVC) material having dimensions of $H \times L \times t$, $1 \times 1 \times 0.01$ m^3, as the host medium. Within the plate, we manufacture a resonant layer with a total height of H_{RL}, composed of a periodic arrangement of square unit cells with a spacing of $a = 0.035$ m, as depicted in Fig. 1(a). Each unit cell, as illustrated in Fig. 1(b), contains an internal resonator that is realized by a cubic steel mass with dimensions $a_r = 0.01$ m and an external casing attached to the host material through four elastic connectors; each connector measures $0.003 \times 0.002 \times 0.002$ m^3. Each cell was directly manufactured in the hosting plate by perforating the plate using a Computer Numerical Control (CNC) machine. The holes created through the perforation process are then used for the realization of resonators by press-fitting the steel cubes inside the plate. The mechanical properties of the considered PVC and steel materials are provided in Table I.

We investigate the dynamics of elastic surface waves polarized in the x–z plane and propagating along the x-direction. Notably, the dispersive law of such edge waves is identical to the one of Rayleigh waves in a half-space, provided that the plate dilatational velocity $c_{L,h} = [E_h/\rho_h(1-\nu_h^2)]^{1/2}$ is used to replace the bulk dilatational wave

velocity of the medium. Here, E_h is Young's modulus, ρ_h is the density, and ν_h is the Poisson's ratio of the PVC material. Given these premises, we designed the experimental setup shown in Fig. 2(a) to characterize the dispersive properties of such surface waves. In particular, we consider three plates, namely (i) a pristine PVC plate (without LRMs) as a reference case, (ii) a plate configuration with three rows of resonators, and another case (iii) with five rows of resonators, as shown in Fig. 2(b). The depths of the resonant layers in cases (ii) and (iii) are approximately $H_{RL} \approx 0.6\lambda_h = 0.105$ m and $H_{RL} \approx \lambda_h = 0.175$ m, respectively. Here, λ_h is the wavelength of the Rayleigh wave at the resonant frequency of the resonators, calculated as $\lambda_h = c_{R,h}/f_r \approx 0.17$ m, where $c_{R,h} = 929$ m/s is the Rayleigh wave velocity in the PVC material. The resonant frequency of the resonators is obtained numerically as $f_r = 5274$ Hz (see Sec. IV A for details).

We position the PVC plate horizontally on an isolated IG Series breadboard table to mitigate any unwanted mechanical vibrations during the measurements. To actuate the surface waves, we utilize a Physik Instrumente P-141.03 piezoelectric transducer (PZT) with dimensions of $0.01 \times 0.01 \times 0.0055$ m^3 and a resonant frequency of 210 kHz, glued to the side surface of the plates. To achieve mechanical excitation in a relatively wide frequency range of interest, a short rectangular pulse of 50 μs duration and an amplitude of 2 V is used.

We note that despite the symmetry inherent in the designed setup, both in terms of excitation and plate sample, which is intended to ensure the decoupling of the in-plane and out-of-plane responses, slight manufacturing discrepancies in the resonators may result in minor coupling. Still, the behavior of the system is well captured by assuming fully decoupled in-plane motion. Therefore, we study the behavior of the LRM layer by measuring the u_z response at several points placed along the x-axis of the plate edge using an Optomet Scanning Laser Doppler Vibrometer (SLDV). The SLDV features an integrated digital signal generator used to actuate the piezoelectric transducer. The generated signal is pre-amplified through a TEGAM 2350 High Voltage Amplifier (hereinafter "signal amplifier"), which provides an output signal amplitude of 200 V. A Tektronix DPO3014 oscilloscope is used in parallel to monitor the input signal. The SLDV is configured with a measurement range of 490 nm, a sampling frequency of 50 kHz, and an average of over ten acquisitions. We utilize a scanning line along the edge of the plates, with a length of $L_{out} \approx 4\lambda_h = 0.8$ m from the sensor, to measure at least four wavelengths of the propagating surface waves at resonance. The scanning step is set to 0.005 m to have sufficient spatial resolution for the calculation of the experimental dispersion relations. Similar setups have been used to investigate the interaction of surface waves with arrays of vertical[7,18] or horizontal[30] surface resonators.

III. DISPERSION ANALYSIS: EXPERIMENTS VS ANALYTICAL RESULTS

Figure 3(a) shows the seismogram generated by the rectangular input pulse propagating as surface waves at the edge of the pristine PVC plate. This seismogram is obtained from the data collected along the acquisition line, indicated as a yellow line in Fig. 2(b). A wavetrain containing a packet of surface waves (SWs) dominates the seismogram. In addition, the back-reflection of the propagating surface waves from the edge of the plate is also visible. We perform a two-dimensional discrete Fourier transform (DFT) on the time waveforms to obtain the dispersion relation (frequency-wavenumber spectrum), as depicted in Fig. 3(d). The spectra of the fundamental surface mode align with the analytical (solid green line) and numerical (green dots) predictions (details are given in Sec. IV).

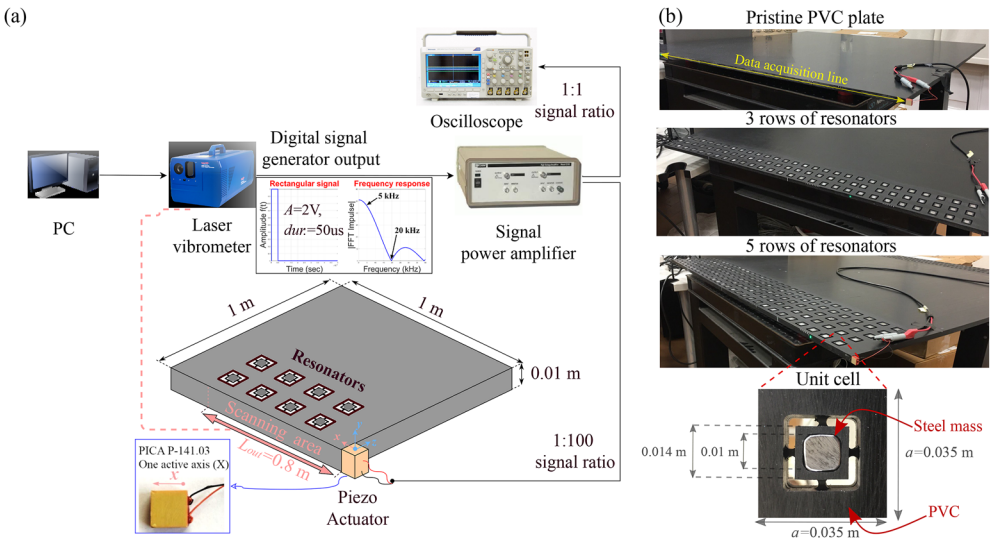

FIG. 2. Experimental characterization of surface waves interacting with thick LRMs. (a) Schematic of the experimental test setup, including a laser Doppler vibrometer and a one-axis piezoelectric actuator; and (b) pristine PVC plate or metamaterial plate with three and five rows of resonators. The inset shows the unit cell with an internal steel mass.

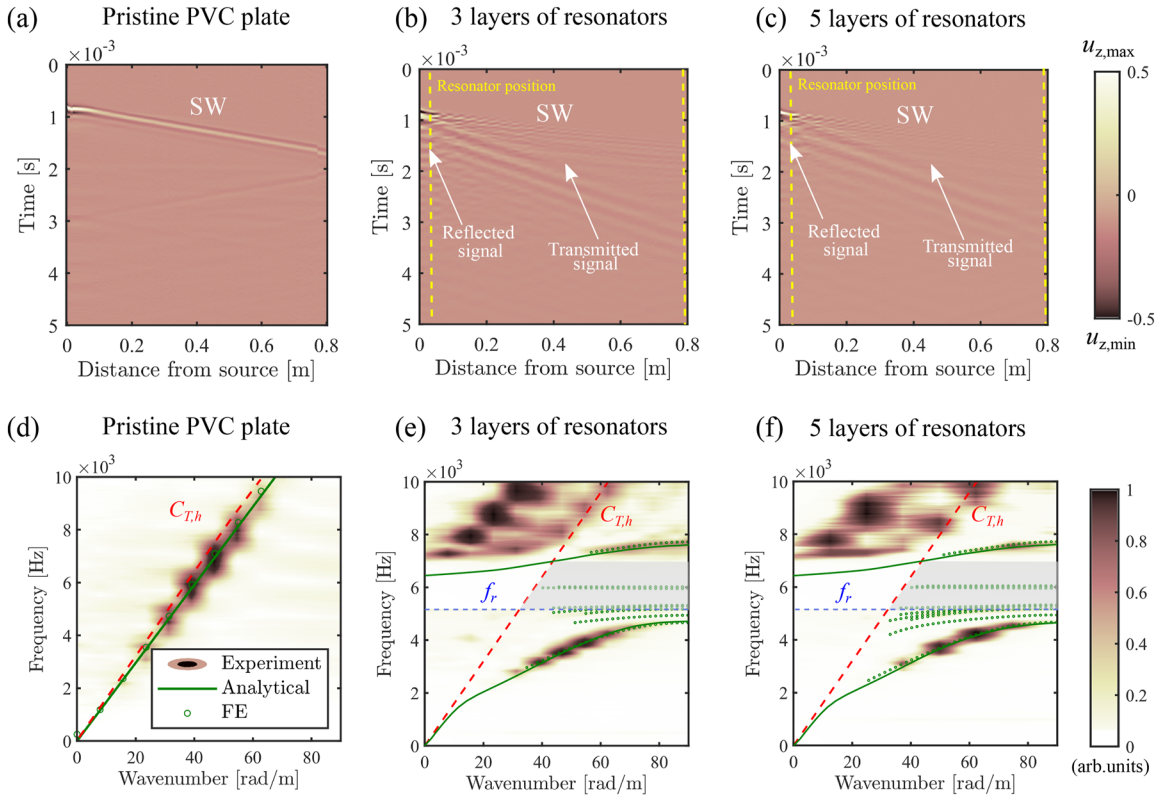

FIG. 3. Top: seismograms of a rectangular pulse propagating in the (a) pristine PVC plate (b) and through a three-layer and (c) a five-layer LRM. Bottom: experimental (dark spots), analytical (green line), and numerical (green dots) dispersion curves of surface mode propagating in the (d) pristine PVC plate and interacting with (e) a three-layer and (f) a five-layer LRM. The gray regions highlight the bandgap zones, and the red and blue dashed lines represent the shear wave speed of the host material ($c_{T,h}$) and the resonant frequency (f_r) of embedded resonators, respectively.

Figure 3(b) illustrates the seismogram generated by an identical pulse propagating in a resonant layer with three rows of resonators embedded below the medium surface, obtained from the same data acquisition line. The two dashed yellow vertical lines indicate the positions of the first and last resonators, respectively. We observe the propagation of new, slower direct, and reflected wavetrains resulting from surface wave scattering by the vertical motion of resonators. We also observe the back-reflection of the pulse when it impinges the first column of resonators.

The corresponding dispersion relation, presented in Fig. 3(e), highlights the existence of two strongly dispersive branches that stem from the interaction between the vertical motion of resonators and the surface wave. The lower branch corresponds to a flat hybrid mode associated, where resonators and host medium move in-phase. This mode asymptotically converges to the resonant frequency of the embedded resonators (f_r, depicted by the dashed blue line). Conversely, the upper branch represents a surface mode where resonators move out-of-phase with respect to the host medium. We use two bandpass filters, one from 0.5 to 5 kHz and the other from 5 to 10 kHz, to better visualize the frequency content of both surface modes. In addition to these surface modes, we observe bulk modes within the sound cone area, the triangular region separated by the shear velocity of the host medium ($c_{T,h}$, dashed red line), where only bulk modes exist.

The existence of the hybridized surface modes well matches the related analytical and numerical predictions. In specific, the upper branch of the hybridized surface modes transforms into a leaky surface mode when its apparent phase velocity falls below the shear velocity of the host material ($c < c_{T,h}$). In this scenario, the mode disperses a portion of its elastic wave energy into the bulk medium [refer to Fig. S5(d) in the supplementary material]. Consequently, the complete surface-to-shear wave conversion phenomena observed in the case of resonant metasurfaces[6,7] do not occur for the resonant layers.[27]

The hybridization mechanism yields a low-frequency bandgap in the frequency interval of $f_{BG,SW} = [5274–7017]$ Hz. In this bandgap region, the surface wave amplitude significantly decreases. The lower edge of the bandgap corresponds to the resonant frequency of the resonators, while the upper edge is determined by the intersection between the out-of-phase branch and the shear wave velocity of the host material.

Similar results are obtained for the case of five rows of embedded resonators. The seismogram for this configuration is shown in Fig. 3(c), and the corresponding dispersion relation is presented in

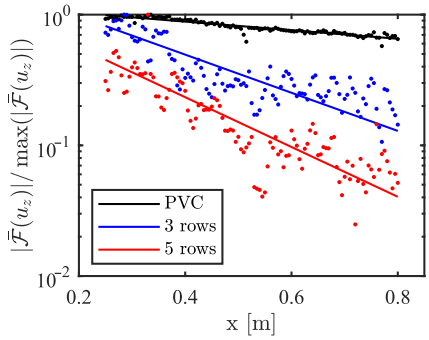

FIG. 4. Surface wave attenuation within the bandgap frequency range. The $\mathcal{F}$ represents the mean DFT of the vertical nodal displacement (u_z). Experimental values are normalized relative to the maximum of each case study. The dots in the figure represent the experimental data, while the continuous lines illustrate the results of exponential fittings.

Fig. 3(f). When introducing two additional rows of resonators, no significant differences are found in the frequency-wavenumber spectrum compared to the configuration with three rows of resonators; however, the bandgap region slightly increases (f_{BG} = [5274–7028] Hz).

We further explore the surface wave attenuation capability of the layered LRMs within the bandgap by estimating the imaginary part of the wavenumber, denoted as k_i. This parameter quantifies the exponential decay of surface wave amplitude in the bandgap region as it propagates along the surface of the resonant layers. For this purpose, signal time traces $u_z(x)$, recorded along the acquisition line, are truncated to remove back-reflections. Then, the mean values of their frequency spectra $\mathcal{F}(u_z(x))$ are computed within the bandgap frequency range. Such mean spectra along the acquisition line x, normalized by their maximum value, are presented in log-scale in Fig. 4. The acquisition is performed between x = 0.2 m and x = 0.8 m to minimize the near-field effects of the source. The figure compares results for the pristine plate and LRMs with three rows and five rows of resonators, marked with black, blue, and red dots, respectively.

We then perform an exponential fit of the form $\mathcal{F}(u_z(x)) = A_F e^{\bar{k}_i x}$ to the experimental data. The fitted results are superimposed on Fig. 4 and represented by solid lines. The coefficients of the exponential provide an estimate of the mean value of the imaginary part of the wavenumber $\bar{k}_i$ within the bandgap region. The estimated values are $\bar{k}_i = -0.7560$, $\bar{k}_i = -3.3599$, and $\bar{k}_i = -4.3860$ for the pristine plate LRMs with three and five rows of resonators, respectively. These values highlight a substantial surface wave attenuation within the bandgap frequency range for the LRMs layer. Interestingly, the surface wave attenuation level is more pronounced when increasing the height of the resonant layer from 3 to 5 rows of resonators.

IV. NUMERICAL AND ANALYTICAL MODELS

This section describes, in brief, the analytical and numerical models used to validate the experimental findings of this study.

A. Analytical dispersion Law

The dynamic interaction between the layered LRMs and surface waves in the long-wavelength regime can be adequately described through the formulation presented in Ref. 27, where a homogenization approach is used to estimate an equivalent continuum of the LRM. This approach aims at defining the properties of an equivalent homogeneous material [see Fig. 1(c)] with frequency-dependent mass density, longitudinal, and shear wave velocities, capable of approximating the dynamic response of the resonant layer in the low-frequency range of interest.

The effective mass density of the unit cell can be calculated by employing a simplified mass-in-mass model of the resonator and host medium.[2] This model results in a scalar and frequency-dependent mass density of $\rho_{eff}(f) = \rho_{st} + \rho_r f^2/(f_r^2 - f^2)$, where f is the frequency, $\rho_{st} = \rho_r + \rho_h$ is the static density of the unit cell obtained at zero frequency, and ρ_r is the mass density of the resonator [see Fig. S3(a) in the supplementary material].

Following the approach in Ref. 27 to calculate the effective longitudinal (M_{eff}) and shear modulus (μ_{eff}) of the LRMs, we develop a 3D finite element model of the unit cell in Comsol Multiphysics.[31] Tetrahedral mesh elements are employed to discretize the model, with a maximum mesh size of $a/30$ = 0.001 m for the connectors and $a/10$ = 0.003 m for the rest of the domain. Under a constrained uniaxial strain state [see Fig. 5(a)], we applied a unitary lateral pressure load on the lateral edges of the unit cell. Through this configuration, we calculate the average stress $\bar{\sigma}_{xx} = \int_V \sigma_{xx} dV/V$ and strain components $\bar{\varepsilon}_{xx} = \int_V \varepsilon_{xx} dV/V$ within the reference host volume (V) to estimate the effective longitudinal modulus $M_{eff} = \bar{\sigma}_{xx}/\bar{\varepsilon}_{xx}$ = 3.13 GPa. Similarly, to compute the effective shear modulus, we impose a unitary horizontal displacement at the top surface of the unit cell and impose continuity conditions along the unit cell lateral boundaries. We then restrain the displacement of the bottom boundary along the horizontal direction [see Fig. 5(b)] and calculate shear stress and strain components. Consequently, we estimate the effective shear modulus $\mu_{eff} = \bar{\sigma}_{xz}/\bar{\gamma}_{xz}$ = 0.47, where $\bar{\sigma}_{xz} = \int_a \sigma_{xz} da \times t/(at)$ and $\bar{\gamma}_{xz} = \Delta u/a$.

After obtaining the effective moduli, the effective longitudinal and shear wave speeds can be achieved as $c_{L,eff}(f) = (M_{eff}/\rho_{eff}(f))^{(1/2)}$ and $c_{T,eff}(f) = (\mu_{eff}/\rho_{eff}(f))^{(1/2)}$, respectively [see Figs. S3(b) and S3(c) in the supplementary material].

We employ the same numerical model to calculate the resonance of the cell by fixing the displacements of the top, bottom, and lateral edges in all directions, as depicted in Fig. 5(c). Due to the symmetry of the unit cell, the vertical and horizontal resonant frequencies are identical and equal to $f_v = f_h = f_r$ = 5274 Hz.

Equipped with the frequency-dependent effective parameters of the homogenized resonant layer, one can derive the dispersion law for the surface wave propagating through an equivalent homogenized layer attached to a non-resonant half-space following the derivations presented in Ref. 27. The dispersion law is presented in matrix form in Eq. (A4) of the Appendix. The dispersion equation can be expressed concisely as $\mathbf{D}(k, f)\mathbf{A} = \mathbf{0}$, where $\mathbf{A}$ represents the amplitude vector and $\mathbf{D}(k, f)$ is a matrix from which its specific components are derived in Eq. (A5). In order to obtain the dispersion relation for the fundamental surface mode in our dynamic system, we set the determinant of $\mathbf{D}(k, f)$ to zero and search for

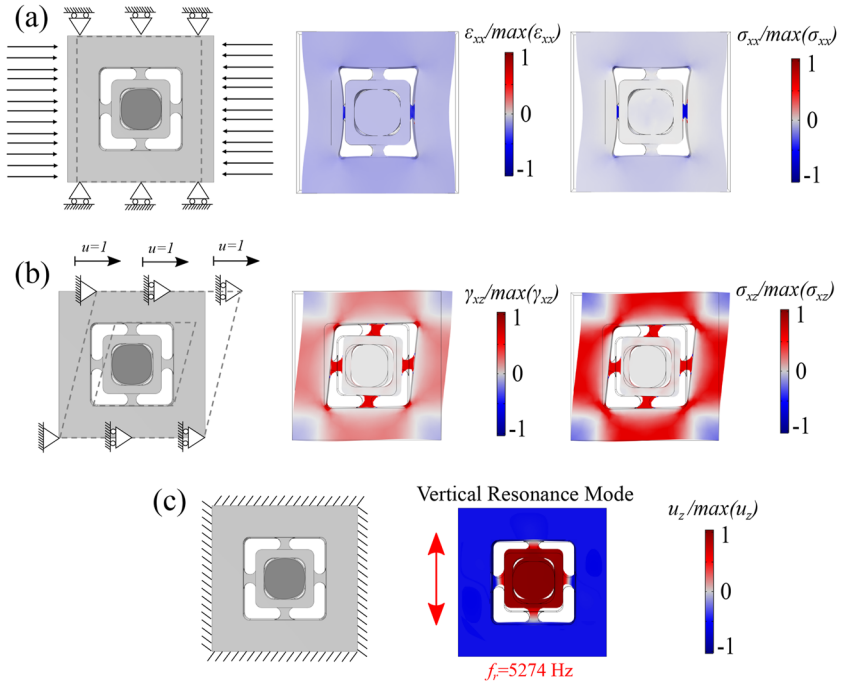

FIG. 5. Schematics of the FE model used to calculate (a) longitudinal modulus (M_{eff}), (b) shear modulus (μ_{eff}), and (c) resonant frequency (f_r) of the LRM.

its non-trivial numerical roots using the Newton–Raphson numerical root-finding scheme. The analytical dispersion relations, indicated by solid green lines in Figs. 3(d)–3(f), perfectly matched the experimental findings, including both repelling branches of the fundamental surface mode.

B. Numerical verification of dispersion relations

To further validate the experimental and analytical findings of this study and to compute the numerical dispersion curves, we exploit the Wave Finite Element Method (WFEM)[32] to develop numerical models in Comsol Multiphysics.[31] The efficiency of this approach has been validated through our previous studies.[9,26,27,30,33] The numerical eigensolutions are superimposed as green dots on the dispersion relations of Figs. 3(d)–3(f), where they encompass a combination of several surface and bulk modes. We use a surface mode selection criterion to distinguish surface modes from bulk ones as follows:[27]

$$Cr = \frac{\int_0^H |u_z| z \, dz}{\int_0^H |u_z| \, dz} < 0.9\lambda_h, \tag{1}$$

where u_z is the displacement field along the z axis. The numerical solutions match both the analytical dispersion law and the experimentally reconstructed dispersive modes for all the examined cases. In addition, the numerical dispersion analysis predicts a few extra flat modes above the resonance and within the LRMs' bandgap frequency range. Further numerical investigations of the full plate model are conducted to reveal the nature of these modes (details are given in Sec. S4 of the supplementary material). The dispersive analysis conducted on the unit cell reveals that such modes are associated with a rotational motion of the embedded resonators, which is neglected in the analytical model. In addition, harmonic numerical analysis aimed at replicating a forced scenario from the PZT source tuned at the propagation frequency of such localized modes (e.g., 5820 Hz) confirms that such modes are not excited by the in-plane motion generated by the source, further confirming the results obtained via the experimental analysis.

V. CONCLUSIONS

We experimentally investigated the dispersive properties of in-plane surface waves propagating in a resonant layer made of embedded resonators overlaying a homogeneous half-space. For this purpose, we designed and manufactured a tabletop setup consisting of a PVC plate embedding a multi-layered array of resonators. The dispersion curves were reconstructed by measuring edge waves along the plate using the laser Doppler vibrometry technique.

The experimentally reconstructed dispersion curves revealed the hybridization of the Rayleigh mode with the collective resonant motion of the resonators. Such coupling yielded the propagation of two distinct surface modes, e.g., an in-phase and an out-of-phase branch, which repel each other and lead to the formation of a resonant bandgap. To quantify the surface wave attenuation within the bandgap, we estimated an average imaginary wavenumber within the bandgap frequency region. This analysis revealed that the deeper resonant layer, realized with five rows of resonators, exhibited a larger attenuation compared to the thinner one, composed of three rows of resonators.

We further interpreted such experimental findings by comparison with the predictions obtained via a recently developed homogenized (analytical) model and an FE model of the setup. The match between analytical, numerical, and experimental predictions confirmed the possibility of modeling the LRM via simplified homogenized models.

Overall, our findings enhance understanding of Rayleigh wave propagation along resonant media and contribute to the development of modeling strategies for the design of deep resonant wave barriers, such as barriers for railway or traffic-induced vibrations.

SUPPLEMENTARY MATERIAL

See the supplementary material for detailed descriptions of experimental data acquisition, signal processing, numerical simulations, and effective parameters (including mass density, longitudinal, and shear bulk wave speeds) of the homogenized LRM.

ACKNOWLEDGMENTS

F.Z. acknowledges funding received from the Italian Ministry of Education, Universities, and Research (MIUR) for the ELeMEnT project under Grant Agreement No. "SOE0000157," CUP: J53C22003890002, under the "Young Researchers Call" of the National Recovery and Resilience Plan (NRRP).

AUTHOR DECLARATIONS

Conflict of Interest

The authors have no conflicts to disclose.

Author Contributions

Farhad Zeighami: Conceptualization (equal); Data curation (lead); Formal analysis (lead); Funding acquisition (lead); Investigation (lead); Methodology (equal); Project administration (supporting); Software (lead); Validation (supporting); Visualization (lead); Writing – original draft (lead); Writing – review & editing (lead). **Antonio Palermo**: Conceptualization (equal); Data curation (supporting); Formal analysis (supporting); Investigation (supporting); Methodology (equal); Supervision (supporting); Validation (lead); Writing – original draft (supporting); Writing – review & editing (supporting). **Denis Bogomolov**: Data curation (supporting); Formal analysis (supporting); Investigation (supporting); Visualization (supporting); Writing – original draft (supporting); Writing – review & editing (supporting). **Alessandro Marzani**: Conceptualization (equal); Funding acquisition (supporting); Methodology (supporting); Project administration (lead); Resources (lead); Supervision (lead); Writing – original draft (supporting); Writing – review & editing (supporting).

DATA AVAILABILITY

The data that support the findings of this study are available from the corresponding author upon reasonable request.

APPENDIX: ANALYTICAL DISPERSION RELATION OF A THICK RESONANT LAYER ATTACHED TO A NON-RESONANT HALF-SPACE

The analytical dispersion law of surface waves propagating in a thick LRM coupled to a homogeneous semi-infinite medium can be obtained by exploiting the dilatation and distortional potential functions that satisfy the wave equations in the resonant layer (RL) and the half-space (HS) after imposing the following boundary conditions:

$$\sigma_{zx,RL} = 0, \quad \sigma_{zz,RL} = 0 \quad \text{for} \quad z = 0, \tag{A1}$$

$$u_{RL} = u_{HS}, \quad w_{RL} = w_{HS} \quad \text{for} \quad z = H_{RL}, \tag{A2}$$

$$\sigma_{zx,RL} = \sigma_{zx,HS}, \quad \sigma_{zz,RL} = \sigma_{zz,HS} \quad \text{for} \quad z = H_{RL}, \tag{A3}$$

namely, zero stress components at the free surface of the resonant layer, Eq. (A1), and continuity of displacements and stresses at the interface between the resonant layer and the half-space, Eqs. (A2) and (A3), respectively. In these equations, σ_{zx} and σ_{zz} represent the horizontal and vertical stress components, while u and w correspond to the vertical and horizontal displacement components. By implementing these dependent boundary conditions, we can reduce the dispersion relation into four independent equations written in matrix form as

$$\mathbf{D}(k,f)\mathbf{A} = \begin{bmatrix} D_{11} & D_{12} & D_{13} & D_{14} \\ D_{21} & D_{22} & D_{23} & D_{24} \\ D_{31} & D_{32} & D_{33} & D_{34} \\ D_{41} & D_{42} & D_{43} & D_{44} \end{bmatrix} \begin{bmatrix} A_1 \\ A_2 \\ A_3 \\ A_4 \end{bmatrix} = \begin{bmatrix} 0 \\ 0 \\ 0 \\ 0 \end{bmatrix}. \tag{A4}$$

The components of the matrix $\mathbf{D}(k,f)$ are the following:

$$\begin{aligned}
D_{11} &= i\left(\cos P - \frac{\delta_1}{\gamma_1}\cos Q\right), \\
D_{12} &= -\frac{\delta_1}{r_1\gamma_1}\sin P - s_1 \sin Q, \\
D_{13} &= -i, \\
D_{14} &= {s_2}^*, \\
D_{21} &= r_1 \sin P + \frac{\delta_1}{s_1\gamma_1}\sin Q, \\
D_{22} &= i\left(-\frac{\delta_1}{\gamma_1}\cos P + \cos Q\right), \\
D_{23} &= -{r_2}^*, \\
D_{24} &= -i, \\
D_{31} &= i\rho_{\text{eff}}\left(r_1\gamma_1 \sin P + \frac{{\delta_1}^2}{s_1\gamma_1}\sin Q\right), \\
D_{32} &= \rho_{\text{eff}}\delta_1(\cos P - \cos Q), \\
D_{33} &= -i\rho_h\gamma_2{r_2}^*, \\
D_{34} &= \rho_h\delta_2, \\
D_{41} &= \rho_{\text{eff}}\delta_1(\cos P - \cos Q), \\
D_{42} &= i\rho_{\text{eff}}\left(\frac{{\delta_1}^2}{r_1\gamma_1}\sin P + s_1\gamma_1 \sin Q\right), \\
D_{43} &= -\rho_h\delta_2, \\
D_{44} &= -i\rho_h\gamma_2{s_2}^*,
\end{aligned} \tag{A5}$$

with the following parameters:

$$
\begin{aligned}
P &= kr_1 H_{RL},\\
Q &= ks_1 H_{RL},\\
\gamma_1 &= 2\left(\frac{kc_{T,eff}}{2\pi f}\right)^2,\\
\delta_1 &= \gamma_1 - 1,\\
\gamma_2 &= 2\left(\frac{kc_{T,h}}{2\pi f}\right)^2,\\
\delta_2 &= \gamma_2 - 1,\\
r_1 &= \sqrt{\left(\frac{2\pi f}{kc_{L,eff}}\right)^2 - 1},\\
s_1 &= \sqrt{\left(\frac{2\pi f}{kc_{T,eff}}\right)^2 - 1},\\
r_2 &= \sqrt{\left(\frac{2\pi f}{kc_{L,h}}\right)^2 - 1},\\
s_2 &= \sqrt{\left(\frac{2\pi f}{kc_{T,h}}\right)^2 - 1},\\
r_2^* &= r_2/i,\\
s_2^* &= s_2/i.
\end{aligned}
\tag{A6}
$$

REFERENCES

[1] Z. Liu, X. Zhang, Y. Mao, Y. Y. Zhu, Z. Yang, C. T. Chan, and P. Sheng, "Locally resonant sonic materials," Science **289**, 1734–1736 (2000).

[2] H. Huang, C. Sun, and G. Huang, "On the negative effective mass density in acoustic metamaterials," Int. J. Eng. Sci. **47**, 610–617 (2009).

[3] N. X. Fang, D. Xi, J. Xu, M. S. Ambati, W. Srituravanich, C. Sun, and X. Zhang, "Ultrasonic metamaterials with negative modulus," Nat. Mater. **5**, 452–456 (2006).

[4] Z. Liu, C. T. Chan, and P. Sheng, "Three-component elastic wave band-gap material," Phys. Rev. B **65**, 165116 (2002).

[5] N. Boechler, J. K. Eliason, A. Kumar, A. A. Maznev, K. A. Nelson, and N. Fang, "Interaction of a contact resonance of microspheres with surface acoustic waves," Phys. Rev. Lett. **111**, 036103 (2013).

[6] A. Colombi, P. Roux, S. Guenneau, P. Gueguen, and R. V. Craster, "Forests as a natural seismic metamaterial: Rayleigh wave bandgaps induced by local resonances," Sci. Rep. **6**, 19238 (2016).

[7] A. Palermo, S. Krödel, A. Marzani, and C. Daraio, "Engineered metabarrier as shield from seismic surface waves," Sci. Rep. **6**, 39356 (2016).

[8] D. Colquitt, A. Colombi, R. Craster, P. Roux, and S. Guenneau, "Seismic metasurfaces: Sub-wavelength resonators and Rayleigh wave interaction," J. Mech. Phys. Solids **99**, 379–393 (2017).

[9] F. Zeighami, L. Sandoval, A. Guadagnini, and V. Di Federico, "Uncertainty quantification and global sensitivity analysis of seismic metabarriers," Eng. Struct. **277**, 115415 (2023).

[10] S. Ouakka, A. Gueddida, Y. Pennec, B. Djafari-Rouhani, G. Kouroussis, and O. Verlinden, "Efficient mitigation of railway induced vibrations using seismic metamaterials," Eng. Struct. **284**, 115767 (2023).

[11] K. Cui, Z.-D. Xu, A. Marzani, and X. Pu, "A multiple scattering formulation to design meta-trenches for mitigating low-frequency ground-borne vibrations induced by surface railways and subways," J. Sound Vib. **562**, 117845 (2023).

[12] S. Yves, R. Fleury, F. Lemoult, M. Fink, and G. Lerosey, "Topological acoustic polaritons: Robust sound manipulation at the subwavelength scale," New J. Phys. **19**, 075003 (2017).

[13] A. Climente, D. Torrent, and J. Sánchez-Dehesa, "Gradient index lenses for flexural waves based on thickness variations," Appl. Phys. Lett. **105**, 064101 (2014).

[14] A. Colombi, S. Guenneau, P. Roux, and R. V. Craster, "Transformation seismology: Composite soil lenses for steering surface elastic Rayleigh waves," Sci. Rep. **6**, 25320 (2016).

[15] M. Martí-Sabaté and D. Torrent, "Edge modes for flexural waves in quasi-periodic linear arrays of scatterers," APL Mater. **9**, 081107 (2021).

[16] X. Pu, A. Palermo, and A. Marzani, "Topological edge states of quasiperiodic elastic metasurfaces," Mech. Syst. Signal Process. **181**, 109478 (2022).

[17] A. A. Maznev and V. E. Gusev, "Waveguiding by a locally resonant metasurface," Phys. Rev. B **92**, 115422 (2015).

[18] A. Palermo, S. Krödel, K. H. Matlack, R. Zaccherini, V. K. Dertimanis, E. N. Chatzi, A. Marzani, and C. Daraio, "Hybridization of guided surface acoustic modes in unconsolidated granular media by a resonant metasurface," Phys. Rev. Appl. **9**, 054026 (2018).

[19] C. Zeng, C. Zhao, and F. Zeighami, "Seismic surface wave attenuation by resonant metasurfaces on stratified soil," Earthquake Eng. Struct. Syn. **51**, 1201–1223 (2022).

[20] L. S. S. Pillarisetti, C. J. Lissenden, and P. Shokouhi, "Control of Rayleigh wave propagation through imposing Mindlin boundary conditions on the surface," J. Sound Vib. **530**, 116931 (2022).

[21] X. Wu, Y. Jin, A. Khelif, X. Zhuang, T. Rabczuk, and B. Djafari-Rouhani, "Topological surface wave metamaterials for robust vibration attenuation and energy harvesting," Mech. Adv. Mater. Struct. **29**, 4759–4767 (2022).

[22] J. M. De Ponti, A. Colombi, E. Riva, R. Ardito, F. Braghin, A. Corigliano, and R. V. Craster, "Experimental investigation of amplification, via a mechanical delay-line, in a rainbow-based metamaterial for energy harvesting," Appl. Phys. Lett. **117**, 143902 (2020).

[23] G. J. Chaplain, J. M. De Ponti, G. Aguzzi, A. Colombi, and R. V. Craster, "Topological rainbow trapping for elastic energy harvesting in graded Su-Schrieffer-Heeger systems," Phys. Rev. Appl. **14**, 054035 (2020).

[24] W. Wang, J. Iglesias, Y. Jin, B. Djafari-Rouhani, and A. Khelif, "Experimental realization of a pillared metasurface for flexural wave focusing," APL Mater. **9**, 051125 (2021).

[25] A. Colombi, R. Zaccherini, G. Aguzzi, A. Palermo, and E. Chatzi, "Mitigation of seismic waves: Metabarriers and metafoundations bench tested," J. Sound Vib. **485**, 115537 (2020).

[26] R. Zaccherini, A. Palermo, A. Marzani, A. Colombi, V. Dertimanis, and E. Chatzi, "Mitigation of Rayleigh-like waves in granular media via multi-layer resonant metabarriers," Appl. Phys. Lett. **117**, 254103 (2020).

[27] F. Zeighami, A. Palermo, and A. Marzani, "Rayleigh waves in locally resonant metamaterials," Int. J. Mech. Sci. **195**, 106250 (2021).

[28] M. V. Wilde, M. V. Golub, and A. A. Eremin, "Experimental and theoretical investigation of transient edge waves excited by a piezoelectric transducer bonded to the edge of a thick elastic plate," J. Sound Vib. **441**, 26–49 (2019).

[29] A. Palermo, Y. Wang, P. Celli, and C. Daraio, "Tuning of surface-acoustic-wave dispersion via magnetically modulated contact resonances," Phys. Rev. Appl. **11**, 044057 (2019).

[30] R. Zaccherini, A. Colombi, A. Palermo, V. K. Dertimanis, A. Marzani, H. R. Thomsen, B. Stojadinovic, and E. N. Chatzi, "Locally resonant metasurfaces for shear waves in granular media," Phys. Rev. Appl. **13**, 034055 (2020).

[31] COMSOL Multiphysics®, "COMSOL AB, Stockholm, Sweden," 2023.

[32] B. R. Mace and E. Manconi, "Modelling wave propagation in two-dimensional structures using finite element analysis," J. Sound Vib. **318**, 884–902 (2008).

[33] F. Zeighami, A. Palermo, and A. Marzani, "Inertial amplified resonators for tunable metasurfaces," Meccanica **54**, 2053–2065 (2019).